

# Numerical Analysis of Hydrodynamic Propeller Performance of LNG Carrier in Open Water

M. Nakisa<sup>a</sup>, A. Maimun<sup>b\*</sup>, Yasser M. Ahmed<sup>a</sup>, Jaswar<sup>a</sup>, A. Priyanto<sup>a</sup>, F. Behrouzi<sup>a</sup>

<sup>a</sup>Faculty of Mechanical Engineering, Universiti Teknologi Malaysia, 81310 UTM Johor Bahru, Johor, Malaysia

<sup>b</sup>Marine Technology Centre, Universiti Teknologi Malaysia, 81310 UTM Johor Bahru, Johor, Malaysia

\*Corresponding author: Adi@fkm.utm.my

## Article history

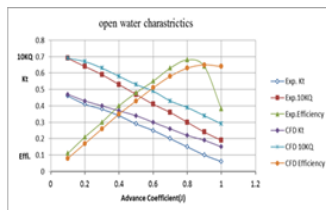
Received :1 July 2013

Received in revised form :

15 July 2013

Accepted :11 December 2013

## Graphical abstract



Hydrodynamic propeller performance  
In open water

## Abstract

Marine propeller blade geometries, especially LNG carriers, are very complicated and determining the hydrodynamic performance of these propellers using experimental work is very expensive, time consuming and has many difficulties in calibration of marine laboratory facilities. This paper presents the assessment on the effect of turbulent model and mesh density on propeller hydrodynamic parameters. Besides that, this paper focuses on the LNG carrier Tanaga class propeller hydrodynamic performance coefficients such as  $K_t$ ,  $K_q$  and  $\eta$ , with respect to the different advance coefficient ( $j$ ). Finally, the results from numerical simulation that were calculated based on RANS (Reynolds Averaged Navier Stocks) equations, were compared with existing experimental results, followed by analysis and discussion sections. As a result the maximum hydrodynamic propeller efficiency occurred when  $j=0.84$ .

**Keywords:** Numerical simulation; LNG carrier; hydrodynamic parameters; propeller; RANS equation

© 2014 Penerbit UTM Press. All rights reserved.

## 1.0 INTRODUCTION

Nowadays, viscid and in-viscid flows with CFD (Computational Fluid Dynamics) are widely used for design aims and the experimental tests to be conducted for the last step of research work. Considering to in maritime applications, numerical methods can be performed to estimate the flow pattern around ship hulls, rudders, propellers and appendages.

In case of the visualisation of flow pattern around merchant ship's propellers, computational fluid dynamics based on Lifting-Surface theory for first step is commonly used [1 and 3]. The viscid RANS (Reynolds Average Navier Stocks) equation solution was used later comes to function after [2].

Reynolds Average Navier Stocks is introduced for the application of numerical technics in fluid mechanics and improvement on computer performances. [4, 6, 7 and 8].

Modelling, geometry, computational domains, boundary conditions, topology, meshing method and mesh size and turbulent method have significant effects on a fruitful numerical analysis and accuracy of simulation. Meshing strategy is divided in two divisions. Hybrid unstructured a mesh means that the tetrahedral elements for flow fluid fields, while structured mesh means that the hexahedral mesh is totally used for meshing on the solid surfaces. In contrast, the results of simulations with structured mesh elements usually have more accuracy than tetrahedral mesh elements results.

Unstructured mesh elements production is almost automatic while hexahedral mesh elements generation is not automatic and should be generated manually. On the other hand, for flow field meshing, sometimes, the geometry is not compatible to use the hexahedral mesh elements, so unstructured mesh elements have better results and convergence of solution is nice. Therefore, we used the hybrid unstructured mesh elements for rotational domain, in which we utilized the stationary and rotational domain for full scale propeller simulation for propeller with five blades.

CFD simulation data were verified with existing tests results. This study focuses on hydrodynamic propeller performance and characteristics in open water condition. The hydrodynamic values such as thrust ( $K_t$ ) and torque ( $K_q$ ) coefficients and the other selected values were measured in this numerical research work.

## 2.0 PROPELLER MODEL

The propeller model with full scale principles was simulated in this numerical work using finite volume method. The diameter ( $D$ ) of considered propeller was 7.7 m and the diameter of hub ( $D_{hub}$ ) was 0.17D, plus the rotation of the propeller was made right handed to make the thrust. Pitch ratio design ( $P/D$ ) was 0.94 and blade ration (EAR) was 0.88.

The propeller drawing is depicted in Figure 1 and the Table 1 shows the geometric characteristics.

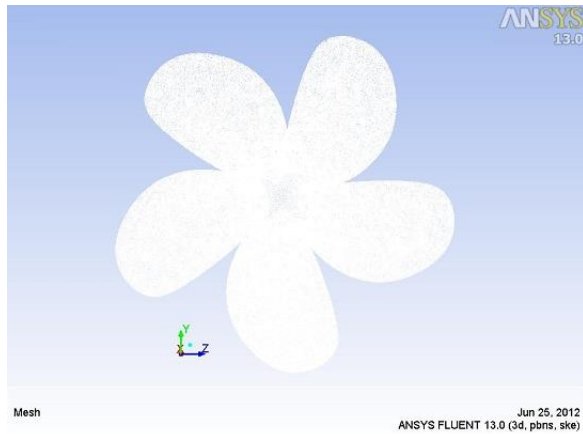


Figure 1 Front view of propeller

The centreline of the propeller was allocated on the centre point and reference of the Cartesian coordination. The x-direction was associated with centreline of the propeller, y-direction was arranged with upward of the propeller and z-direction followed the right handed Cartesian coordination system that showed to port side, as shown in Figure 1.

Table 1 Propeller geometric characteristics

Parameters	Dimension
Z	5
D	7.7 m
Dhob	1.28 m
Br	0.17
P/D	0.94
Ae/A0	0.88
R	15 Deg.

3.0 BOUNDARY CONDITION

ANSYS-Fluent 13 was applied to numerical prediction of the hydrodynamic propeller characteristics which solved the RANS equation by finite volume method. Figure 2 and Table 2 show the scheme and dimensions of computational domain to simulate the propeller in open water, respectively.

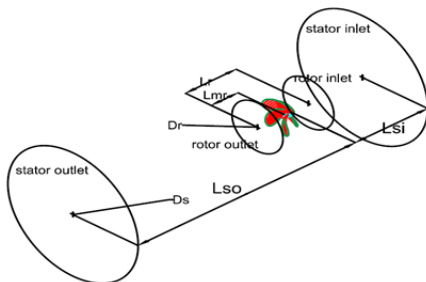


Figure 2 scheme of computational domain

Multiple Frame of Reference (MRF) was applied in the numerical estimation of the flow around the ship propeller

technique. In accordance to uniform and homogeneous flow around the ship propeller, mathematical predictions were done focusing on total blades, similarly.

Table 2 Dimensions of computational domain

Value	Rotational	Stationary
Dr	1.44 D	
Lmr	1.5 D	
Lr	3 D	
Ds		10 D
Lsi		3 D
Lso		5 D
d		1.7 D

The stationary and rotating parts are called stationary and rotating, respectively. Table 2 shows the characteristics of the domain of propeller: D is the propeller diameter and L<sub>mr</sub> is the axial length of outlet in rotational domain, as shown in Figure 2. It was considerable to remove the wall effect on results. The dimensions of boundaries were considered far enough from the propeller in the stationary part. Figure 3 shows the suitable distance for domains.



Figure 3 Rotational and stationary domain

4.0 NUMERICAL METHOD

In Cartesian tensor form the general RANS equation for continuity can be written as,

$$\frac{\partial \rho}{\partial t} + \frac{\partial(\rho u_i)}{\partial x_i} = 0 \tag{1}$$

and equation for momentum become:

$$\begin{aligned} \frac{\partial(\rho u_i)}{\partial t} + \frac{\partial(\rho u_j u_i)}{\partial x_j} = & \\ - \frac{\partial \rho}{\partial x_i} + \frac{\partial}{\partial x_i} [\mu (\frac{\partial u_i}{\partial x_j} + \frac{\partial u_j}{\partial x_i} - \frac{2}{3} \delta_{ij} \frac{\partial u_l}{\partial x_l})] + & \\ \frac{\partial}{\partial x_i} (-\rho \overline{u_i' u_j'}) + f_{bi} & \end{aligned} \tag{2}$$

In the above equation  $u_i$  is  $i^{\text{th}}$  Cartesian component of total velocity vector,  $\mu$  is molecular viscosity,  $(-\rho \overline{u_i' u_j'})$  is Reynolds stress,  $\delta_{ij}$  is Kronecker delta and  $p$  is static pressure. The

Reynolds stress should be demonstrated to near the governing equations by suitable turbulent model. For solution the RANS equation and turbulence velocity time scale, it is used by Boussinesq's eddy-viscosity supposition and two transport equations. The body force is expressed by  $f_{bi}$ .

For determination the 3D viscous incompressible flow around the ship's hull is used the ANSYS-CFX14.0 code. The parallel version of CFX concurrently calculates the flow formulations using numerous cores of computers. The shear stress transport (SST) turbulence model had been used in this study, because it gave the best results in comparison with other turbulence models. The equations are shown as follows:

Equation of  $k$  :

$$\frac{\partial}{\partial t}(\rho k) + \frac{\partial}{\partial x_i}(\rho k u_i) = \frac{\partial}{\partial x_j}(\Gamma_k \frac{\partial k}{\partial x_j}) + G_k - Y_k + S_k \quad (3)$$

Equation of  $\omega$ :

$$\frac{\partial}{\partial t}(\rho \omega) + \frac{\partial}{\partial x_i}(\rho \omega u_i) = \frac{\partial}{\partial x_j}(\Gamma_\omega \frac{\partial \omega}{\partial x_j}) + G_\omega - Y_\omega + S_\omega \quad (4)$$

Where  $G_k$  and  $G_\omega$  express the generation of turbulence kinetic energy due to mean velocity gradients and  $\omega$ .  $\Gamma_k$  and  $\Gamma_\omega$  express the active diffusivity of  $k$  and  $\omega$ .  $Y_k$  and  $Y_\omega$  represent the dissipation of  $k$  and  $\omega$  due to turbulence.  $D_\omega$  expresses the cross-diffusion term,  $S_k$  and  $S_\omega$  are user-defined source terms Further detail is available in [9].

5.0 RESULT AND DISCUSSION

Figures 4 and 5, show the distribution of pressure coefficient on face and back surface of one blade at three radial section  $r/R = 0.80$ . It is clearly that the low pressure region is happen on back surface and the high pressure region is occurred on face surface of blade.

It is clearly that the low and high pressure regions are occurred on back and face surfaces of blades, respectively.



Figure 4 Contours of pressure coefficient on blade section

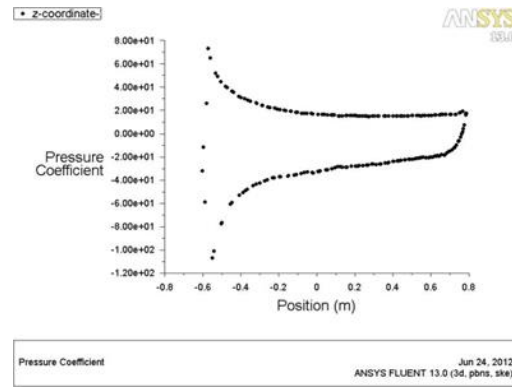


Figure 5 Pressure coefficient distribution on back and face surfaces of blade section

Also, the Figure 6 shows that the distribution of low pressure and high pressure area (static pressure) on back and face surface of 5 blades, respectively. The positive pressure face of each blades make positive force to push the propeller x direction that called thrust propeller.

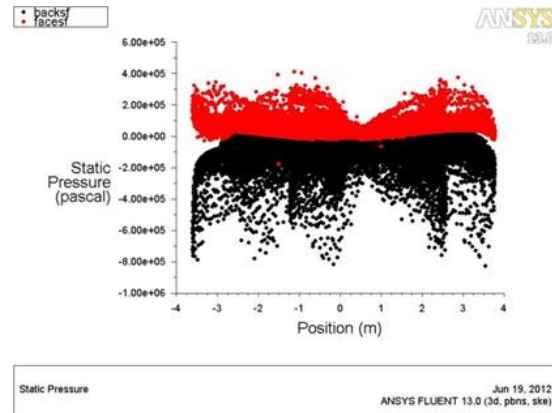


Figure 6 Distribution of static pressure on face and back surfaces of 5 blades

When the propeller rotate around (x)-direction, generate thrust in (+x)-direction and high pressure occurs on face surface and low pressure on back surface of blades, respectively. [see Figures 7 and 8]. Figure 9 shows the contours of total pressure behind the propeller.

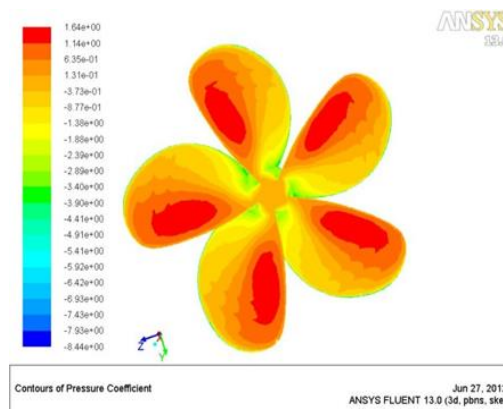


Figure 7 Contours of pressure coefficient on face surface

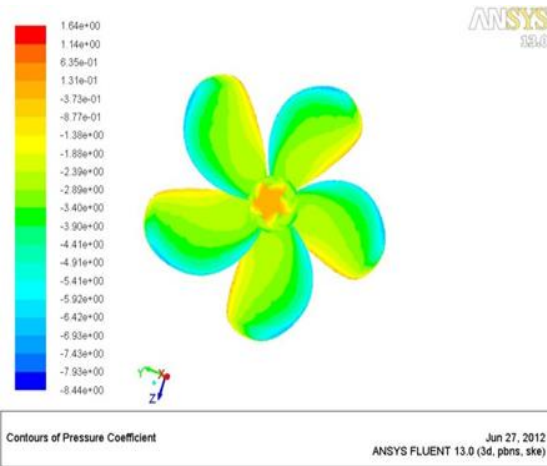


Figure 8 Contours of pressure coefficient on back surface

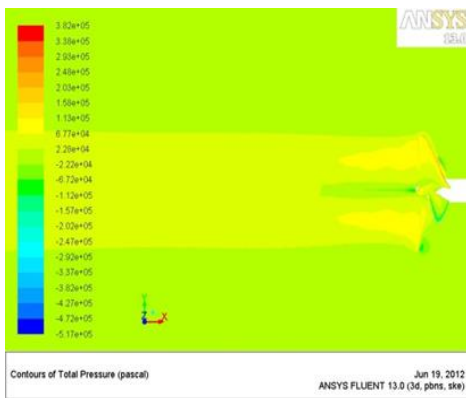


Figure 9 Contours of total pressure behind the propeller

Figures 10-12, show the Contours of velocity magnitude behind the propeller, contours of velocity magnitude on face surface and velocity magnitude vectors behind the propeller, respectively. The velocity magnitude in tip of blades is higher than other region of blade surfaces. Because of the higher rotation in tips of blades, the momentum of fluid particles is very higher than near hub.

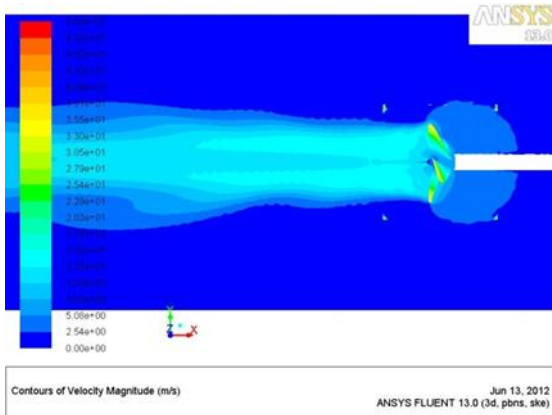


Figure 10 Contours of velocity magnitude behind the propeller

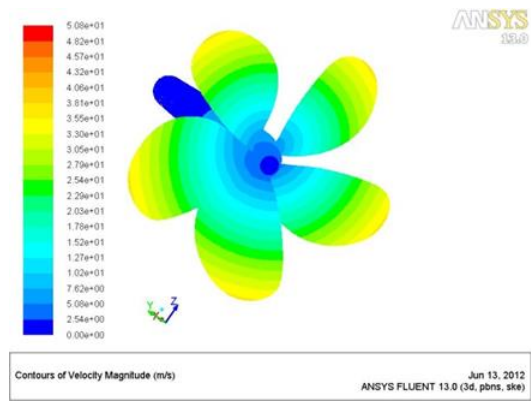


Figure 11 Contours of velocity magnitude on face surface

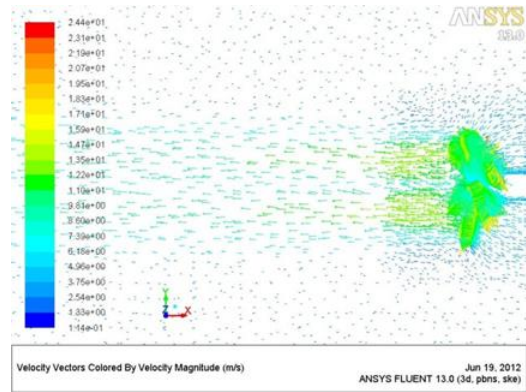


Figure 12 Velocity magnitude vectors behind the propeller

### 6.0 PROPELLER PERFORMANCE

Due to the propeller model of LNG carrier has been used in experimental and numerical simulation; some similarity criteria should be applied to approach the similar results to compare the real propellers.

A series of non-dimensional specifications are used to show moments and forces that produced by propellers as followings:

$$\text{Thrust coefficient: } k_t = \frac{T}{\rho n^2 D^4} \tag{5}$$

$$\text{Torque coefficient: } k_q = \frac{Q}{\rho n^2 D^5} \tag{6}$$

$$\text{Advance coefficient: } J = \frac{V_a}{nD} \tag{7}$$

The results from the Numerical simulation of propeller in open water based on RANS equation of LNG ship’s propeller at full scale compared to the model test results can be seen in Figure 13. Various J-values are obtained by keeping a same revolutions (n=108rpm) but varying the flow speed. The trends of results with varying advance ratio are well predicted. It should be noted that  $K_Q$  and  $K_t$  are slightly over predicted all the way. The maximum hydrodynamic propeller efficiency will be occurred in  $j=0.84$ .

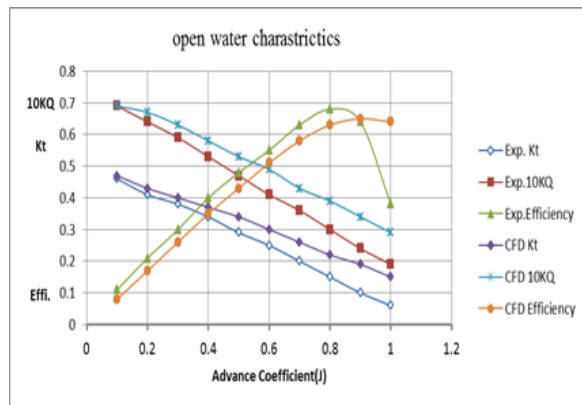


Figure 13 Propeller characteristics in open water

## 7.0 CONCLUSION

Nowadays, numerical methods have been improved to estimate the flow field around the propellers and their hydrodynamics performance.

RANS (Reynolds-Averaged Navier-Stokes) methods have become a useful tool in flow analysis, engineering design and optimization. They open up new possibilities in analysis and comprehension of flow phenomena which are impossible or difficult to be implemented using traditional model tests. In accordance to the presented computational results based on RANS equations, the following conclusions are drawn:

- The propeller worked in a uniform fluid stream, producing the forces and moments, therefore, it generated the thrust and produced velocity and pressure on face blades surface and behind the propeller in the fluid flow.
- The fluid velocity in the tips of face blades was higher than other areas and the fluid pressure in the face blades near leading edges was higher than other areas.
- The maximum hydrodynamic propeller efficiency occurred when  $j=0.84$ .

## Nomenclature

- $D$  : Propeller diameter, (m)
- $D_{hub}$  : Hub diameter, (m)
- $Z$  : Number of blade
- $P/D$  : Pitch Ratio
- $R$  : Rake of Blades
- $N$  : Rate of revolutions of propeller, (rpm)
- $C_p$  : Pressure coefficient
- $P$  : Static pressure at point of interest
- $p_0$  : Reference pressure at infinity
- $V_a$  : Advance velocity, (m/s)

- $J$  : Advance ratio
- $K_T$  : Thrust coefficient
- $K_Q$  : Torque coefficient
- $Br$  : Boss ratio
- $A_E/A_0$  : Expanded Area Ratio (EAR)
- $\rho$  : Density of water
- $\eta$  : Open water efficiency
- $D_r$  : Diameter of Rotational domain
- $L_r$  : Length of rotational domain
- $L_{mr}$  : Outlet length of rotational domain
- $D_s$  : Diameter of stationary domain
- $L_{so}$  : Length of outlet stationary domain
- $L_{si}$  : Length of inlet stationary domain
- $(x, y, z)$  : Cartesian coordinate system with its origin at the centre of propeller
- $+X, +Y, +Z$  : Cartesian directions in Right-Hand system
- $U_x, U_y, U_z$  : Velocity components in the Cartesian coordinate system  $(x, y, z)$

## Acknowledgements

The authors would like to express their sincere gratitude to Universiti Teknologi Malaysia (UTM) for financial support given to this research work.

## References

- [1] Kerwin, J. E. and C.S. Lee. 1978. Prediction of Steady and Unsteady Marine Propeller Performance by Numerical Lifting-Surface Theory. *Trans SNAME*. 86(4): 218–253.
- [2] Kim, H. T. and F. Stern. 1990. Viscous Flow Around a Propeller-shaft Configuration with Infinite-pitch Rectangular Blades. *J. Propul.* 6: 434–443.
- [3] Streckwall, H., 1986. A Method to Predict the Extent of Cavitation on Marine Propellers by Lifting-surface-theory. *International Symposium on Cavitation*. Sendai, Japan
- [4] Abdel-Maksoud, M., F. Menter and H. Wuttke. 1998. Viscous Flow Simulations for Conventional and High-skew Marine Propellers. *Schiffstechnik/Ship Technol. Res.* 45: 64–71.
- [5] Watanabe, T., T. Kawamura, Y. Takekoshi, M. Maeda and S.H. Rhee. 2003. Simulation of steady and unsteady cavitation on a marine propeller using a RANS CFD code. *5<sup>th</sup> International Symposium on Cavitation (CAV2003)*. Osaka, Japan
- [6] Chen, B. and F. Stern. 1999. Computational fluid dynamics of four-quadrant marine-propulsor flow. *J. Ship Res.* 43(4): 218–228.
- [7] Oh, K.-J. and S. H. Kang. 1992. Numerical Calculation of the Viscous Flow Around a Rotating Marine Propeller. *KSME J.* 6(2): 140–148.
- [8] Kawamura, T., Y. Takekoshi, H. Yamaguchi, T. Minowa, M. Maeda, A. Fujii, K. Kimura and T. Taketani, 2006. Simulation of unsteady cavitating flow around marine propeller using a RANS CFD code. In: *6th International Symposium on Cavitation (CAV2006)*, Wageningen, The Netherlands.
- [9] Fluent 6.2 User's Manual. 2005. Ansys.